Copyright

by

Matthew Robert Gonzales

2011

The Report Committee for Matthew Robert Gonzales
Certifies that this is the approved version of the following report:

Engineering a Compliant Muscle Joint for Dynamic Locomotion in Very Rough Terrain

APPROVED BY
SUPERVISING COMMITTEE:

Supervisor:

Luis Sentis

Benito Fernandez

Engineering a Compliant Muscle Joint for Dynamic Locomotion in Very Rough Terrain

by

Matthew Robert Gonzales, B.S.

Report

Presented to the Faculty of the Graduate School of

The University of Texas at Austin

in Partial Fulfillment

of the Requirements

for the Degree of

Master of Science in Mechanical Engineering

The University of Texas at Austin

December 2011

Acknowledgements

I would like to thank my supervising professor Dr. Luis Sentis for providing me the opportunity to be involved in humanoid robotics. It was truly an eye opening experience navigating through the breadth and depth of the subject with your guidance. I appreciate all the patience and assistance you have provided me throughout my academic journey.

I dedicate this report to my parents. Without their constant support, many of my accomplishments would not have been possible.

Abstract

Engineering a Compliant Muscle Joint for Dynamic Locomotion in Very Rough Terrain

Matthew Robert Gonzales, MSME

The University of Texas at Austin, 2011

Supervisor: Luis Sentis

In humanoid robotics, there is a long pursuit of making bipeds capable of walking in highly unstructured and roughly sensed environments. Within this goal, our objective is to develop a compliant bipedal humanoid robot, based on McKibben pneumatic actuators that can move in these terrains as well as quickly adapt to unpredicted variations on the contact state. We present here the first part of our work, focusing on the design, construction and control of a pneumatic robotic joint capable of achieving the control performance necessary for responding compliantly and accurately to contact transitions while delivering high forces needed to handle the physical challenges associated with rough terrains. In particular, we address our progress in the mechanical and embedded electronic design, actuator modeling, and compliant control strategies for a robotic joint based on fluidic pneumatic artificial muscles (PAMs). The proposed robotic joint has been validated experimentally, exploring various aspects of its performance as well as its shortcomings, but overall demonstrating the potential benefits of using pneumatic muscles.

Table of Contents

List of Figures vii

I. INTRODUCTION **8**

II. BACKGROUND AND EARLIER WORK **10**

III. MECHANICAL AND EMBEDDED DESIGN **12**

A. Mechanical design 12

B. Embedded electronics 15

IV. ACTUATOR MODELING AND CONTROL **16**

A. Model 16

B. Controller 21

V. DYNAMIC LOCOMOTION IN VERY ROUGH TERRAIN **24**

A. The proposed algorithm 24

VI. EXPERIMENTAL RESULTS **27**

VII. CONCLUSIONS **32**

Bibliography 33

List of Figures

Figure 1: Human-size research biped robot for advanced locomotion. 8

Figure 2: Mechanical and embedded design of the pneumatic joint. 13

Figure 3: Modeling of a PAM. 14

Figure 4: BondGraph of the PAM model. 18

Figure 5: Bond Graph of the antagonism structure.. 20

Figure 6: Neuro-Bond-Graph used to characterized the PAM. 21

Figure 7: Block diagram of low-level compliant controller. 23

Figure 8: Data extraction from human walk 26

Figure 9: Automatic locomotion planner. 27

Figure 10: Behavior of the robot leg against impact forces 28

Figure 11: Force/Torque control 30

Figure 12: Gravity Compensation. 31

I. INTRODUCTION

In the near future, it may become ubiquitous for humanoid robots to interact with and among their human partners, by adopting technologies to take on the "burden of adaptation"[1]. Because these types of robots interact closely with humans, attention must also be given to safety requirements as well as the traditional metrics of performance [2]. For this study, we take a Human Centric design approach, the primary purpose of which is to create robots that are safe and skillful when interacting with humans and among human environments. Moreover, biped robots offer a less intrusive, more natural appeal to humans (see Figure 1 for a concept illustration of our biped robot).

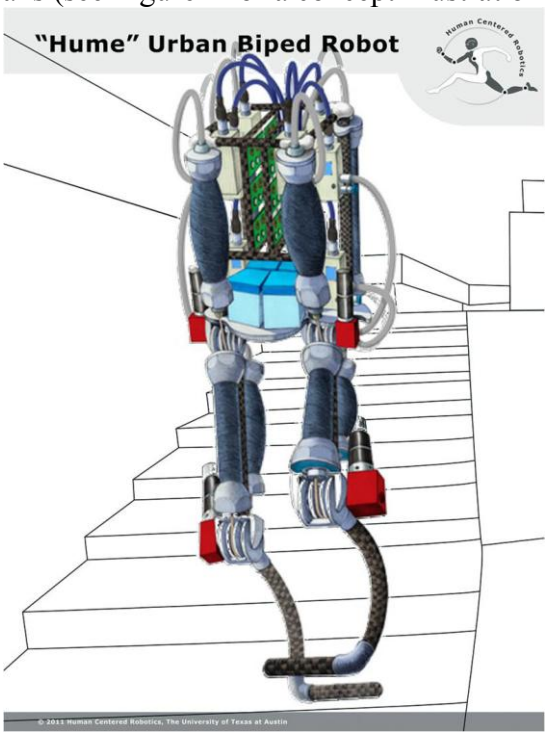

Figure 1: Human-size research biped robot for advanced locomotion.

Currently, most of the robotic legs use electrical motors due to the maturity of the technology and the accuracy of motors. However, they present important drawbacks such

as moderate weight-force ratio, high friction and high reflected inertia [3]. These effects become especially apparent when using high gear ratios necessary for rough terrain locomotion. Motivated by these limitations, there is a growing interest in developing new actuators with human like capabilities. One example is the pneumatic muscle, particularly, the McKibben type actuator. This device provides an interesting and potentially very promising alternative as an actuation source for bipedal walking. However, there are two main drawbacks that need to be overcome [4]: (a) Modeling errors: the current models are not detailed enough to effectively control the system, and (b) Low bandwidth of the actuators: they are considered too slow for many robotic applications, especially in the area of locomotion. In particular, locomotion over rough terrain requires fast and smooth placement of the feet.

In this work we present our ongoing progress in the areas of mechanical and embedded system design, as well as actuator modeling and control. In particular, we present the design and control of a robotic joint using Bond Graphs [5]. The proposed mechanism will be part of a future compliant bipedal humanoid robot, shown in Figure 1, capable of implementing advanced planning and control strategies necessary to maneuver in difficult urban and back terrains. For this purpose, an effective torque controller has been developed and implemented showing an adequate force response in terms of accuracy. This controller also provides the ability to carry out accurate position control through a force interface, which is basic for impedance regulation to adapt to the environment during contact transitions. Finally, this paper also describes a new dynamic locomotion algorithm for very rough terrain that could be used for planning the dynamic maneuvers.

The remainder of this paper goes as follows. First, the background and earlier work is presented in Section II; later, we discuss the Mechanical and Embedded Design

in Section III; we then describe the Actuator Modeling and Control in Section IV; fourth, we present a new algorithm designed for bipedal locomotion (Section V), while the experimental results that demonstrate the performance of the muscle system are shown in Section VI. Finally, we discuss the pros and cons as well as future work of the robotic joint (Sec. VII).

II. BACKGROUND AND EARLIER WORK

Modern design of biped robots using artificial muscles can be attributed to Kato [6] during the late sixties and the seventies. Work on pneumatic legs continued with [7], where the authors presented a biped robot called Lucy. This comprehensive work was centered in the development of a full anthropomorphic lower body using pleated pneumatic artificial muscles (which have different dynamic characteristics than McKibben muscles; for instance, they do not display friction or hysteresis). In [8], the mechanical structure of a robotic inferior limb mechanism was presented. Positions could be controlled but not the interaction forces exerted by the muscles. Also, in [9], a complex biped robot actuated by pneumatic muscles (24 in total) was developed but was lacking a control strategy all together. In [10], a biped robot driven by antagonistic pairs of McKibben pneumatic muscles was also presented. It could change joint compliance according to the desired locomotion pattern by applying a bang-bang controller using solenoid valves with two outputs (on-off). However, they did not consider the dynamic model of the muscle. In [11], the authors reported the development of an oscillator controller for bipedal robots with antagonistic pairs of pneumatic actuators. They proposed a mechanical architecture with a simple timing controller that enabled the robot to walk robustly in flat terrains. Recently, [2] introduced a manipulator robot with 2 DOF and four pneumatic muscles and proposed the addition of an independent stiffness

controller so that the manipulator's position and compliance could be controlled simultaneously. For modeling the robot arm they used the work of Reynolds [12]. In [13], the authors presented an antagonistic pneumatic joint, carrying out a control strategy based on the model by [14]. They also developed a new solenoid valve to control the pressure of the Mckibben muscles, allowing them to increase the bandwidth of the actuator to 3 Hz.

With respect to modeling, Caldwell and others [15], proposed the use of a simple model of a Pneumatic Muscle Actuator (PMA) that could determine the relation between force and pressure. Later, Chou and Hannaford [16] developed an analytic model where the constant friction force that opposes the motion of the muscle and the bearing on output forces due to the braid's thickness were considered. In [17], a model that used a damped Gauss-Newton estimator was proposed. Tondu et al [14] proposed a model based on the virtual work principle. In [18], the forces exerted by the latex tubing in terms of circumferential stretch and longitudinal compression were considered. Davis et al [4] proposed a new model where the actuator stress was taken into account. In [19], a parameter-based strategy that modifies the contraction ratio was proposed. Also in [19], a new model that introduced the effect of air flow for pressure variance was studied. This model allowed the authors to obtain good results for the estimation of the input pressure and the resulting joint angle, but not for the delivered output force. Other models based on numerical methods can be found in [15], [20], [21].

Control strategies depend on the type of model that the authors use. In [15], the authors proposed an adaptive control scheme that switched between various position control laws. In [22] and [23], a linear PID was proposed but it achieved poor tracking. In [14], the authors used fuzzy control strategies. In [24] and [25], the authors developed sliding mode controllers. In [26], a nonlinear PID control using neural network was

proposed. Finally, a sliding mode controller was proposed in [27] to control the position of a linear stage using two PMAs.

III. MECHANICAL AND EMBEDDED DESIGN

The context of the ongoing project is the design of a bipedal robot to demonstrate the capabilities of rough terrain locomotion. Our lab is aggressively pursuing this objective and at the same time slowly building a robust design methodology that will allow us to leverage the current results. As a first step we have designed a single powerful joint based on the principle of co-contraction. The objective is to demonstrate the ability to control with force and position feedback heavy loads while maximizing the bandwidth of the joint (for an illustration of the design of the joint see Figure 2).

A. Mechanical design

The proposed joint employs fluidic artificial muscles consisting of a bladder that inflates with air and a deformable mesh that generates large contraction forces. The appealing characteristics of fluidic muscles are their elastic capabilities and their relatively high strength to weight ratio. A muscle of 4[cm] diameter and 30[cm] length can exert a theoretical maximum force of 6,000[N] at full extension and up to 2,000[N] when contracted 20% of its full length. Another positive feature is their relatively high commercial availability.

Based on a human centric approach, the main objective of our design is to create a lightweight human-like anthropomorphic biped robot that is both skillful at locomotion and adaptive to the environment. We complement our approach with the biomechatronics methodology, in this case by looking at characteristics of the human body during jumping behaviors. In such movements, the human knee exerts the highest amount of forces, with

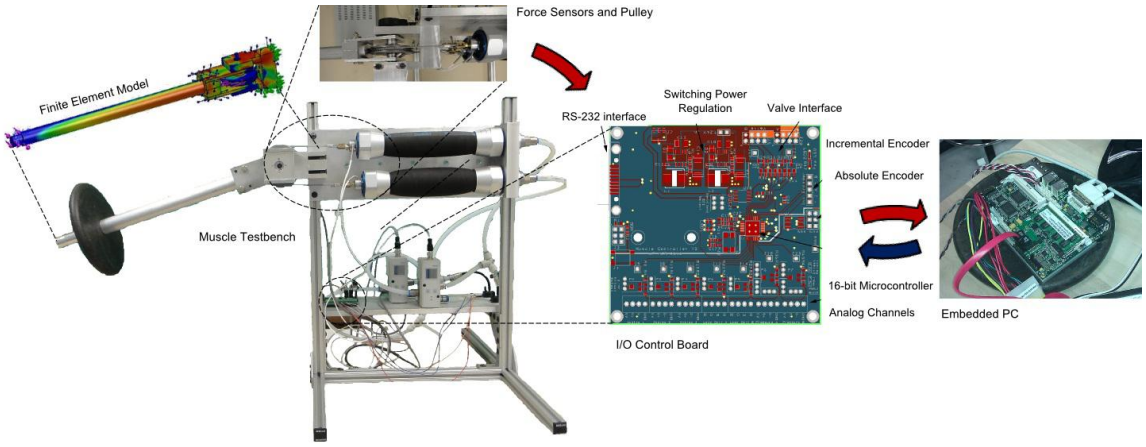

Figure 2: Mechanical and embedded design of the pneumatic joint.

peak torques reaching as high as 400[Nm] upon accelerating upwards (i.e. during knee extension) [28]. Also, during multi-contact interactions elevated torques might appear during extreme dynamic maneuvers like free-running or jumping. We are currently researching a variety of possibilities in terms of the target skills, but it seems reasonable to take jumping as a nominal high force scenario. Several contributions in jumping maneuvers using artificial muscles have been made by the group cited on [10].

The human quadriceps muscle group of healthy humans can exert up to 7,000[N] of static force during squatting [29]. If we add the contribution of inertial accelerations during jumping, these forces exceed this value. In comparison, the forces exerted by commercial artificial muscles such as those of Festo can top realistic values up to 2,000[N]. Therefore, because in the first design presented here we use a single muscle per direction of movement of the joint, we cannot expect to reach torques as high as those of humans. A second tradeoff to take into consideration is due to the contraction limit of the muscles. Because commercial artificial muscles are able to contract only about 20% of their total length, it is desirable to create articulations with a small radius. However, in

doing, so we lose torque output. Therefore, in the designs of joints using artificial muscles there is a difficult tradeoff between number of muscles per joint, torque capability, range of movement, length of the muscle, and weight of the leg. In the design of Fig. 3 we take into consideration only torque capabilities and operating range of motion. In particular we target to achieve performance values inferior than those of the human knee, with maximum torques of 80[Nm] and range of motion of 70[deg]. A choice for this design specification gives us a pulley radius of 4[cm]), i.e.

if $\tau = 80$ [Nm], $F = 2000$ [N], then $r = \frac{\tau}{F} = 4$ [cm],

and length of the muscle of 25[cm], i.e.

if $\theta = 70$ [deg], $h = 20\%$, then $l = 5\theta r = 25$ [cm].

Figure 2 shows the benchmark setup designed and built to test the robot joint. The figure shows a finite element analysis (FEA) simulation carried out to test the maximum forces that can be exerted by the joint, as well as the mechanical and electronic setup.

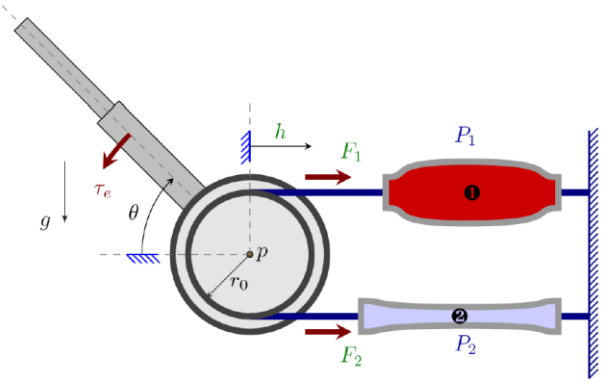

Figure 3: Modeling of a PAM: The main components are the two bladders (1) and (2), each exerting forces F_1 and F_2 in co-contraction. Both joints move (in opposite directions) a distance h that rotate the joint (radius r_0) at an angle about the pivot p.

B. Embedded electronics

In order to achieve our goal of developing a bipedal robot for rough terrain locomotion, it is necessary to fully understand all layers of the system [30]. To be practical, a robotic hardware system must fulfill the requirements of openness, adaptability, interoperability and plug-and-play extensions [31]. For these purposes, we have chosen a controller for the antagonistic muscle based on a two tier cascaded system. Control originates at a desktop computer which handles most of the computational workload and provides a user-friendly developer interface. The host machine communicates with the designed embedded system through a RS-232 serial link. Control commands pass from the host to the embedded system in the form of messages containing controller set points, such as the desired pressures. The embedded system then operates on these control set-points and responds to the host system with an update of the system's sensory output. The sensors include knee position and both pressure and force for each muscle. Knee position is measured using an incremental encoder. Muscle force is measured by a load cell attached in series with each muscle. Internal muscle pressure is measured by the Festo proportional valve that controls the air flow on the muscles.

For real-time (RT) control purposes the software used by the host computer is Matlab's Realtime Workshop which uses the Realtime Windows Target (RTWT) library. In later stages of the project we will switch to a full realtime operating system on an embedded PC (see Figure 2) and use a 'Whole Body Controller' as the system's central controller.

IV. ACTUATOR MODELING AND CONTROL

The artificial muscle joint consists of two McKibben type bladders that we connect in an antagonistic fashion as shown in Figure 3. We first look at a single muscle and model its behavior.

A. Model

The air behavior in a muscle can be described assuming an ideal gas law:

$$PV^{\gamma} = mR_aT \text{ [kg/mol])} = 287.1 \text{ [J/kg·K]}, \quad (1)$$

where, m is the total mass of air inside the bladder, T is the air temperature in [°K], γ is the adiabatic index that depends on whether the process is adiabatic ($\gamma = C_p/C_v$) or not (γ =1), C_p is the specific heat for constant pressure, C_v is the specific heat for constant volume, $R_a = R/\mu_a = 287.1$[J/kg·K] is the air gas constant, $R = 8.3145$[J/mol·K] is the universal gas molar constant, and $\mu_a = 0.02896$[kg/mol] is the molecular weight of air.

The best case scenario for the bladder dynamics is a reversible, isothermal expansion. It would allow the largest amount of available energy to be stored. The worst scenario is an adiabatic expansion, which assumes the gas expands so quickly that no heat energy is absorbed from the environment. Normally, for this type of systems, the amount of energy provided by the air supply will be between the adiabatic and isothermal behaviors. In this case, equation (1) can be transformed to:

$$PV^{\gamma-1} = \rho R_aT, \quad (2)$$

where ρ is the air density. Multiplying both terms by the volumetric flow rate, Q (BG flow variable), and noting that $\dot{m} = \rho Q$, we have:

$$PQV^{\gamma-1} = \dot{m}R_aT. \quad (3)$$

Here, $\dot{m}$ can be controlled with the inlet and outlet valves.

On the other hand, taking the time derivative of Eq. (1), and considering that the process is isothermal (i.e. T is constant), we obtain:

$$\dot{P}V + P\dot{V} = \dot{m}R_aT. \quad (4)$$

Then, using Eqs. (3) and (4), we define the relationship:

$$\dot{P}V + P\dot{V} = \frac{PQ}{\rho}, \quad (5)$$

where, the right term represents the energy introduced to the muscle. Equation (5) represents the energy stored in the bladder ($\dot{P}V$) and the energy transmitted to the mechanical element ($P\dot{V}$).

In order to model the PAMs, we propose to use BondGraphs [32], [33], [34], [35], [36]. Applying BG to the PMA, we obtain the model described in Figure 4. This figure shows the model of the McKibben-type PAM as a multi-domain storage element and could not have been modeled as a simple (lumped) BG element. It simultaneously stores energy in the pneumatic and mechanical domains. In other words for a given displacement h (Figure 3), if more air is forced into the bladder, it acts as a pneumatic capacitor: the pressure P will increase depending on the mass inside the bladder, m which deforms the shape of the elastic bladder to a volume V. Energy is stored in the compressed air as well as in the elastic mesh of the bladder. These coupled relations are represented in BG by capacitive fields, $\mathbb{C}$. In our system, we model two actuators, $\mathbb{C}_u$ for the "upper" bladder and $\mathbb{C}_l$ for the "lower" bladder. The mappings can be described by the output equations:

$$\begin{bmatrix} F_u \\ P_u \end{bmatrix} = \begin{bmatrix} \Phi_{F_u}(L_u, V_u) \\ \Phi_{P_u}(L_u, V_u) \end{bmatrix} = \mathbb{C}_u^{-1}(L_u, V_u) \quad (6)$$

$$\begin{bmatrix} F_l \\ P_l \end{bmatrix} = \begin{bmatrix} \Phi_{F_l}(L_l, V_l) \\ \Phi_{P_l}(L_l, V_l) \end{bmatrix} = \mathbb{C}_l^{-1}(L_l, V_l) \quad (7)$$

where, V_j and L_j correspond to the volume and length (related to h in Fig. 3) of each bladder ($j = \{u,l\}$ for upper and lower subcomponent) –dynamic states of the system–, F_j

corresponds to force that each bladder exerts on its muscle, and P_j is the internal pressure of the bladders (again, $j = \{u,l\}$ for upper and lower subcomponents).

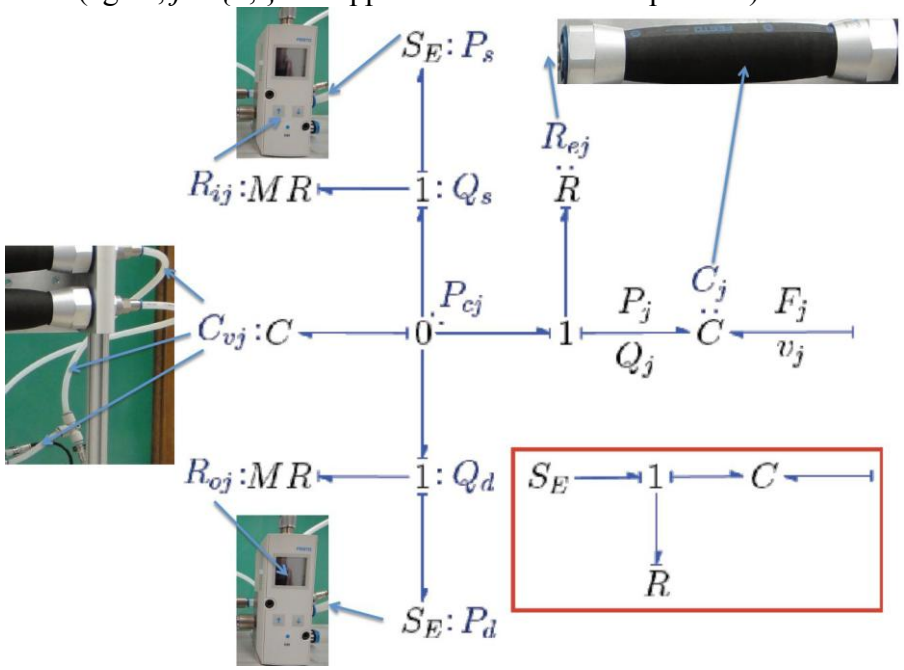

Figure 4: BondGraph of the PAM model: The model includes the inlet and outlet air regulators that feed the muscle's bladder. The bladder is modeled as a capacitive field ($C : Cj$) with two ports, the left that provides the fluidic interface (to the air regulator) and the right to the mechanical (translational) interface (to the actuator mechanism, F_j in Fig. 3). The inner chamber of the regulator has capacitance behavior (C_{vj}) and three ports attached to it: inlet from a regulated ($MR : R_{ij}$) supply, P_s; outlet, also from regulated ($MR : R_{oj}$) discharge, P_d; and the conduit to the bladder (with its own resistance, R_{ej}). The insert (red square) represents the closed loop pressure-controlled simplification of the model.

Figure 4 shows the model of the muscle that includes the pressure controller. In the figure, the pressure supplied is modeled by an effort source ($S_E : P_s$), so is the air discharge ($S_E : P_d$). Since the pressure is regulated, a degree of freedom is reduced. The bond graph expresses the force pressure-position relationship as the constitutive relation of a capacitive field. The simplified model enclosed in a red box represents the power

delivered to the actuator, with some of its power stored in the capacitor C – in the form of compressed air – and the rest transmitted through the piston.

Using BGs we can easily obtain a full representation of the dynamics of the muscles as shown in Fig. 5. From the previous Bond Graph of the actuator, we add two BGs on the left side of the Figure, each PAM contributing with a force F_u and F_l (or F_1 and F_2 in Fig. 3) that, through the pulley, generate a net torque to the load. From the BG, we extract the PAMs nonlinear dynamic equations:

$$\dot{V}_u = \frac{1}{R_{eu}} \left(P_{cu} - \Phi_{P_u}(L_u, V_u)\right) \quad (8)$$

$$\dot{L}_u = r_u \frac{h_L}{J_L} = r_u \omega_L = v_u \quad (9)$$

$$\dot{V}_l = \frac{1}{R_{el}} \left(R_{cl} - \Phi_{P_l}(L_l, V_L)\right) \quad (10)$$

$$\dot{L}_l = r_l \frac{h_L}{J_L} = r_l \omega_L = v_l \quad (11)$$

$$\dot{h}_L = r_u \Phi_{F_u}(L_u, V_u) - r_l \Phi_{F_l}(L_l, V_l) \quad (12)$$

where, the system's state is represented by the energy variables V_j and L_j, corresponding to volume and length of the bladders respectively, (j = {u,l} for upper and lower subcomponents), and h_L represents the angular momentum of the loaded limb. The R_{ej}'s represent pneumatic resistances of the bladder supply (from the pressure regulators, P_{cj}'s), the r_j's represent radii of the muscle connections to the actuator joint, the v's represent the actuators linear velocities, and ω_L represents the angular velocity of the joint. The nonlinear mapping of the air muscles is characterized by $\Phi_{Fj}(L_j, V_j)$.

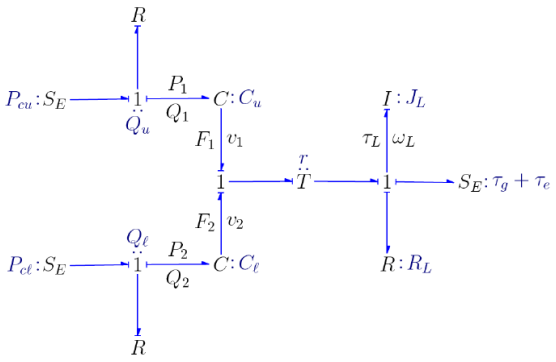

Figure 5: Bond Graph of the antagonism structure. The left side shows the upper (subindex *u*) and lower (subindex *l*) PAMs, each with a regulated pressure P_{cu} and P_{cl}. Each muscle is modeled by a capacitive field (C_u and C_l) as described in Fig. 4. On the right side of the C-fields, the two wires are attached to the pulley (Fig. 3), shown in the BG as a transformer ($T : r$) with modulus *r*. The rest of the BG (on the right) represents the rotational mechanical inertia, J_L, with frictional resistance, R_L, and a source of effort, S_E that combines the gravitational effects, τ_g, and external loads, τ_e.

To fully characterize the antagonist muscle joint, we use Neuro-Bond-Graphs (NBGs) [37], [38], [39]. NBG is a technique that allows the use of a priori knowledge about a system by creating a "gray-box" recurrent neural model, generating a sparse network from a Bond Graph. In many engineering systems, we have a pretty good idea of what the system dynamic model looks like and usually there might be few components with unknown characteristics. In fact, in many instances, researchers turn to general models (ARX, ARMA, NNets, Fuzzy, etc.) because of their simplicity, but at the same time, the models represent a "black box" in the sense that, after "tuning" the model, little is known about the system's component characteristics. The resulting tool, called Neuro-Bond-Graph (NBG) generates a sparse network from a Bond-Graph (BG). NBG represents a quantum improvement over conventional approaches, because it incorporates knowledge acquired through the enhanced pattern recognition capabilities of neural networks and the physical information about the system provided by BondGraphs.

The network implements a causal form of Equations (8–12) where the unknown mappings (namely, $\Phi_{Fj}(L_j\ ,\ V_j)$) are realized by three-layer perceptrons (3LP) embedded in the recurrent NNet (DyNet [40]). Figure 6 shows the NBG as used to characterize the constitutive relations of the bladders.

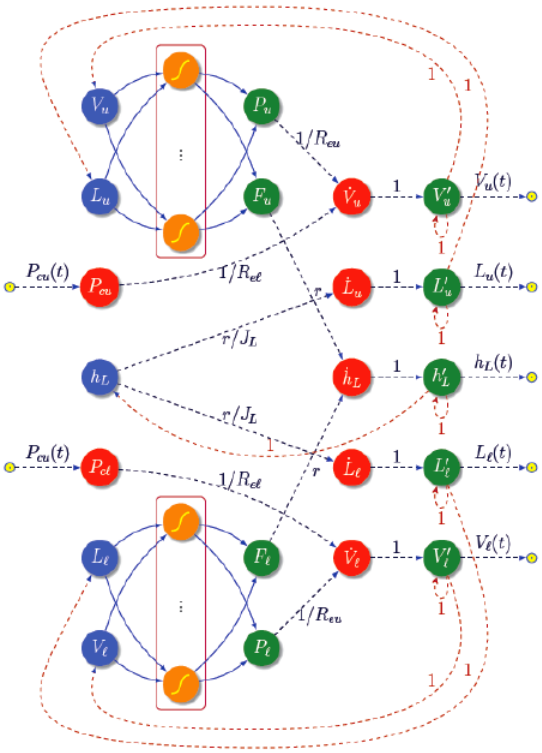

Figure 6: Neuro-Bond-Graph used to characterize the PAM. The equations (8–12) are used to generate a sparse recurrent NNet (DyNet) that captures the system dynamics functionality (especially causality). The unknown parameters or functions are learned by the DyNet from experimental data.

B. Controller

Equations (6) and (7) represent nonlinear mappings from length and volume states (L_j, V_j) to force and pressure outputs (F_j, P_j). The pressure regulator controls the pressure by controlling the amount of volumetric flow of air in and out of the bladder. So volume is tied to pressure. Then, instead of having two mappings, $F_j = \Phi_{Fj}(L_j,\ V_j)$ and $P_j = \Phi_{Pj}(L_j,$

V_j), we can use the latter mapping to find V_j from L_j and P_j (i.e., $V_j = \Phi_{P_j}^{-1}(L_j, P_j)$) and substitute it in the first mapping, resulting in a quasi-static relation between pressure and length to force,

$$F_j = \Psi_{F_j}(L_j, P_j) = \Phi_{F_j}(L_j, \Phi_{P_j}^{-1}(L_j, P_j)) \quad (13)$$

This is a key dynamic relation that can be used for impedance and torque control. For an effective length of the muscle we can use this relation to determine the pressure required (P_{rj} in Fig. 7) for the muscle to provide a desired force (F_{jr} in Fig. 7),

$$P_{rj} = \Psi_{P_j}(L_j, F_j) = \Psi_{F_j}^{-1}(L_j, F_j) \quad (14)$$

Having presented the model of the joint we now focus on the controller. Since our focus is on force control, we propose the control-loop presented in Fig. 7, which consists on: (a) an internal nonlinear PID control loop that regulates the pressure inside each bladder, (b) a hybrid feed-forward term that uses the mapping extracted from the Neuro-Bond-Graph (Eq. 14) to feed-forward the quasi-static pressure expected to generate the desired force, and (c) an additional feedback force controller that uses the difference error between the force reference, $F_{jr}(t)$, and the sensed force of each PAM, F_j. The force reference comes from the outer-loop generated by the Task Planner module, that uses the sensory input ($F_j(t)$;$L_j(t)$) and the scheduled path to generate the immediate reference force.

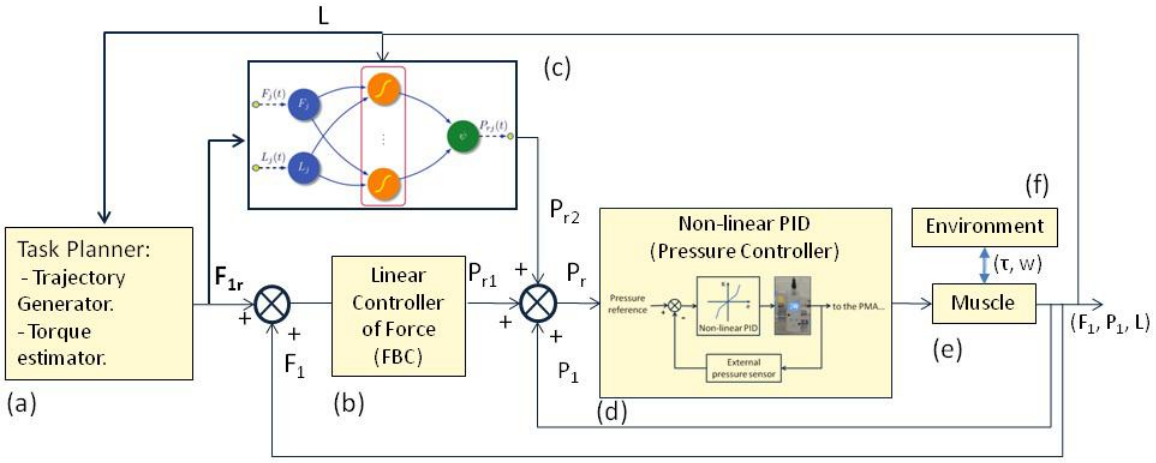

Figure 7: Block diagram of low-level compliant controller: The control strategy consists of two nested feedback loops and a feed-forward branch. (a) Provides the desired force reference which is produced by a feedback trajectory or force policy (not shown here). (b) Implements a PID controller for fast motion. (c) Implements the neural network of the quasi-static mapping between the bladder length and desired force to the steady-state pressure. The relation of Eq. (14) characterizes each bladder of the PAM. The functional mapping is learned from experimental data. (d) Shows the inner feed-forward pressure loop for the bladder (1). (e) Corresponds to the muscle plant. (f) Depicts the interaction between the muscle and the environment with τ_e being the external torque applied.

The nonlinear PID was designed as a gain-scheduler to compensate the delay variation of the pneumatic system with the operating point and implemented in discrete-time. As it can be seen in the experimental results, the closed-loop behavior shows improved performance (faster bandwidth and smaller tracking error). Given that we have two antagonistic muscles, we have an extra degree of freedom that we have used to implement a stiffness controller. In this dual controller, we can specify position or (net) force of the end-effector and the perceived passive stiffness of the system. For torque/force control, what is needed is the net force applied by the PAMs, $F_{net} = F_1 - F_2$. As such, there are an infinite number of combinations of F_f's that would provide F_{net}. The additional degree of freedom is used to control the passive stiffness of the system,

$$K_j = \frac{\partial F_j}{\partial L_j} = \frac{\partial \Psi_{F_j}(L_j, P_j)}{\partial L_j} = K_j(P_j, L_j) \quad (15)$$

$$K_{eff} = K_1(P_1, L_1) - K_2(P_2, L_2) \quad (16)$$

where, K_{eff} represents the effective stiffness of the system as perceived by the environment and K_j's are the local stiffness of each PAM (j). Note that as L_1 increases, L_2 decreases by the same amount, ($L_1 + L_2$ = constant). We can see in Eq. (13) that given the nonlinear relation between P_j, L_j, and F_j, we can take advantage of the nonlinearity to change the relative pressures, P_j's in order to vary K_{eff}.

V. DYNAMIC LOCOMOTION IN VERY ROUGH TERRAIN

We have developed a new algorithm for dynamic locomotion in very rough terrain which has been recently submitted for publication. It is based on the hypothesis that center of mass (CoM) state manifolds can be created using perturbation theory and then used to find contact transition states to produce dynamic walking in very rough terrains.

Only a few successful attempts have tackled the problem of locomotion in moderately uneven terrain. Our take on this problem is therefore an important step to bring biped robots outside of the lab. In dynamic walking we can classify techniques in the following categories: Trajectory based techniques derived from the Zero Moment Point (ZMP) criterion [41], Prediction of contact placement [42] and Limit cycle based techniques [43] or Hybrid methods [44].

A. The proposed algorithm

Our approach, called cascading manifolds, can be explained in terms of various phases: (1) pre-conditioning, (2) CoM state-space manifold-based solver, (3) post-conditioning, and (4) optimization. Since our algorithm is not presented in this paper, we

will only explain phase 2. The CoM state-space manifold-based solver consists on: (1) formulating acceleration manifold due to contact state, (2) taking into account unconstrained vertical variations, (3) conversion to state-space, (4) cascading neighboring manifolds, and (5) extraction of vertical manifolds. Using a human-size robot model, we consider a variable stepped terrain with height variations between ±40 [cm] and width variations between 30-40 [cm] (see Figure 9). The goal of the planner is to maneuver the robot through the total length of the terrain. The speed specifications are determined to cruise the terrain at an average speed of 0.6 [m/s]. We also assume that the robot starts and finishes with zero velocities and it increases velocity through the steps according to a trapezoidal profile. Velocity specifications are given only at each new step, corresponding to the moment when the center of mass sagittal position crosses the corresponding supporting foot, namely the apex of the step. Steps are therefore defined to be the span from apex to apex.

For every contact state, we formulate dynamic equilibrium of moments. This relationship yields a well-known solution that relates sagittal accelerations with respect to center of mass sagittal and vertical distances to contact locations, and with the latter multiplied by vertical accelerations plus gravity. Most researchers simplify the above equation by assuming fixed vertical CoM and feet conditions. However, to walk in very rough uneven terrains this assumption is no longer valid. Instead, we assume unconstrained vertical CoM and feet variations, assuming they will be kinematically and dynamically feasible. Using perturbation theory we obtain the incremental relationship between CoM positions and velocities for each contact state, thus yielding state-space CoM specifications. Because we operate in state-space we remove time as a variable. The CoM manifolds, by construction, describe the CoM behavior before and after each apex. If we combine neighboring manifolds, the transition state can be determined finding the

intersection of the curves. Using the prescribed CoM kinematic path, it is now possible to extract the corresponding CoM manifold in the vertical direction. Moreover, given the contact transition states it is also possible to derive feet state-space curves. This information in turn, can be utilized to create joint velocity or torque feedback controllers to make the CoM manifold an attractor.

Preliminary results have been performed at the Human Centered Robotics Lab and consist of comparing the locomotion of a human subject (see Figure 8) with that of the proposed automatic CoM planner (see Figure 9) using only kinematic information from the human. The results demonstrate a strong correlation of CoM behavior between the human and the planner.

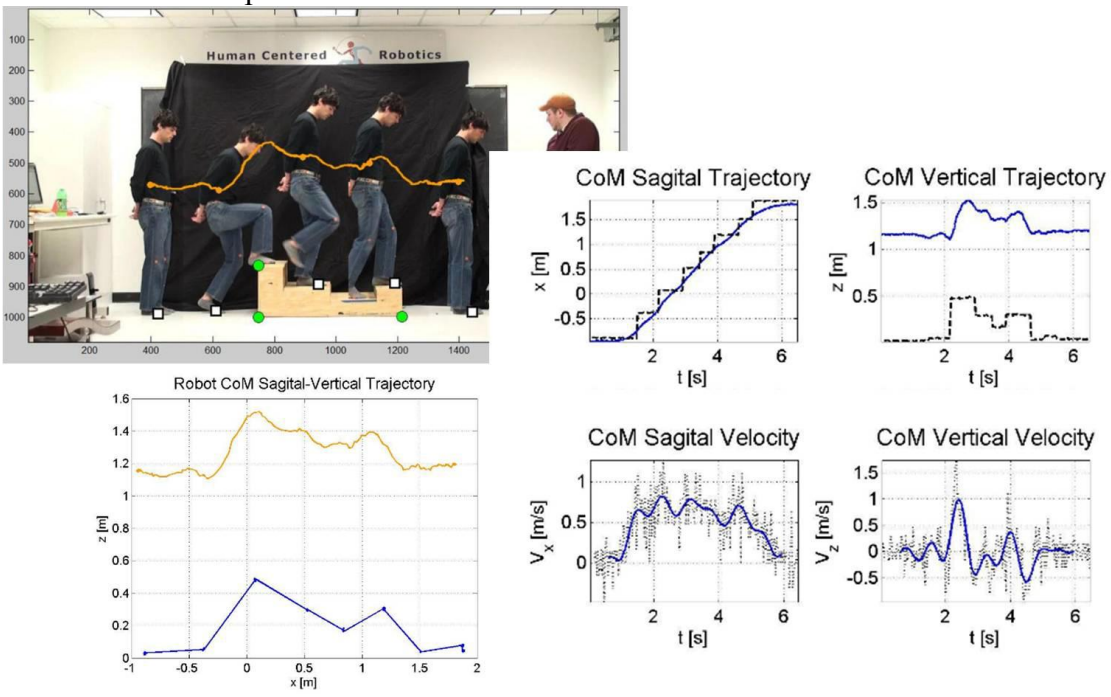

Figure 8: Data extraction from human walk: A human subject walks over a rough terrain. Marker tracking is implemented and used to extract approximate CoM paths as well as sagittal and vertical CoM trajectories and velocities.

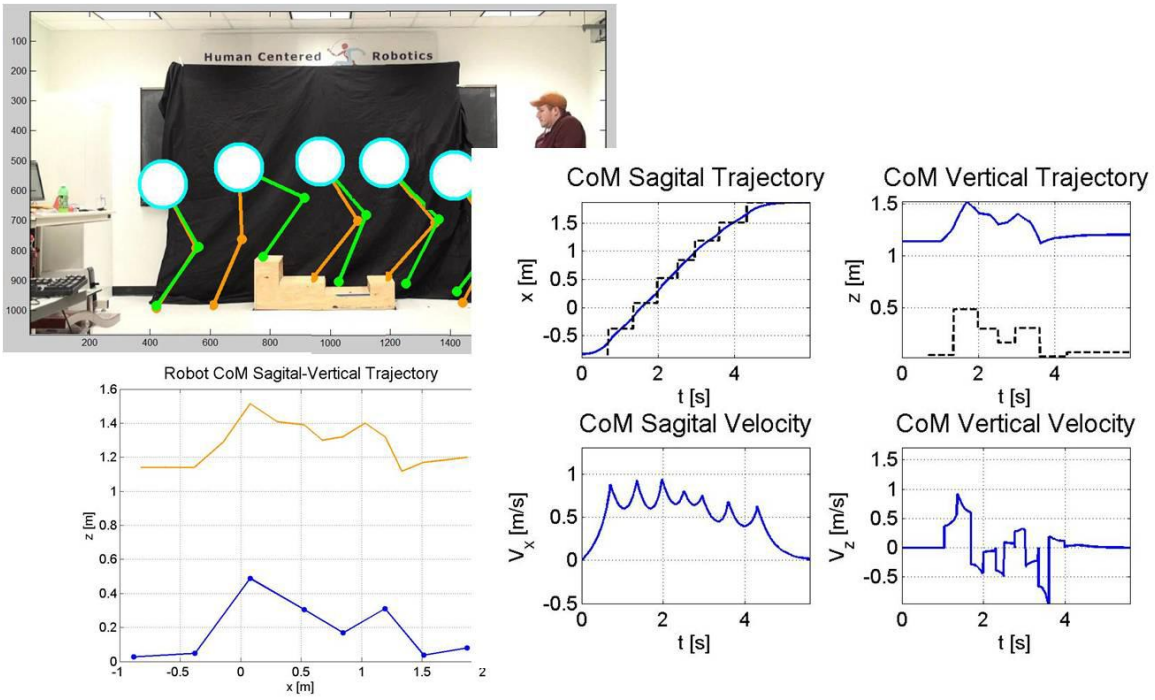

Figure 9: Automatic locomotion planner: Using the proposed locomotion planner and based on human kinematic data, we create artificial CoM trajectories and determine contact transitions to achieve the desired design specifications of the walk.

VI. EXPERIMENTAL RESULTS

We have conducted different experiments to validate various aspects of the compliant joint. Note that these experiments were carried out on the joint prototype, evoking the final behavior of the bipedal robotic system. These are:

1) Study of the behavior of the Robot Leg against impact forces.

2) Position control through a force interface.

3) Force tracking and torque control.

4) Gravity compensation.

At the end of this section, we review the first experiments that were done for calculating the locomotion of the bipedal robot.

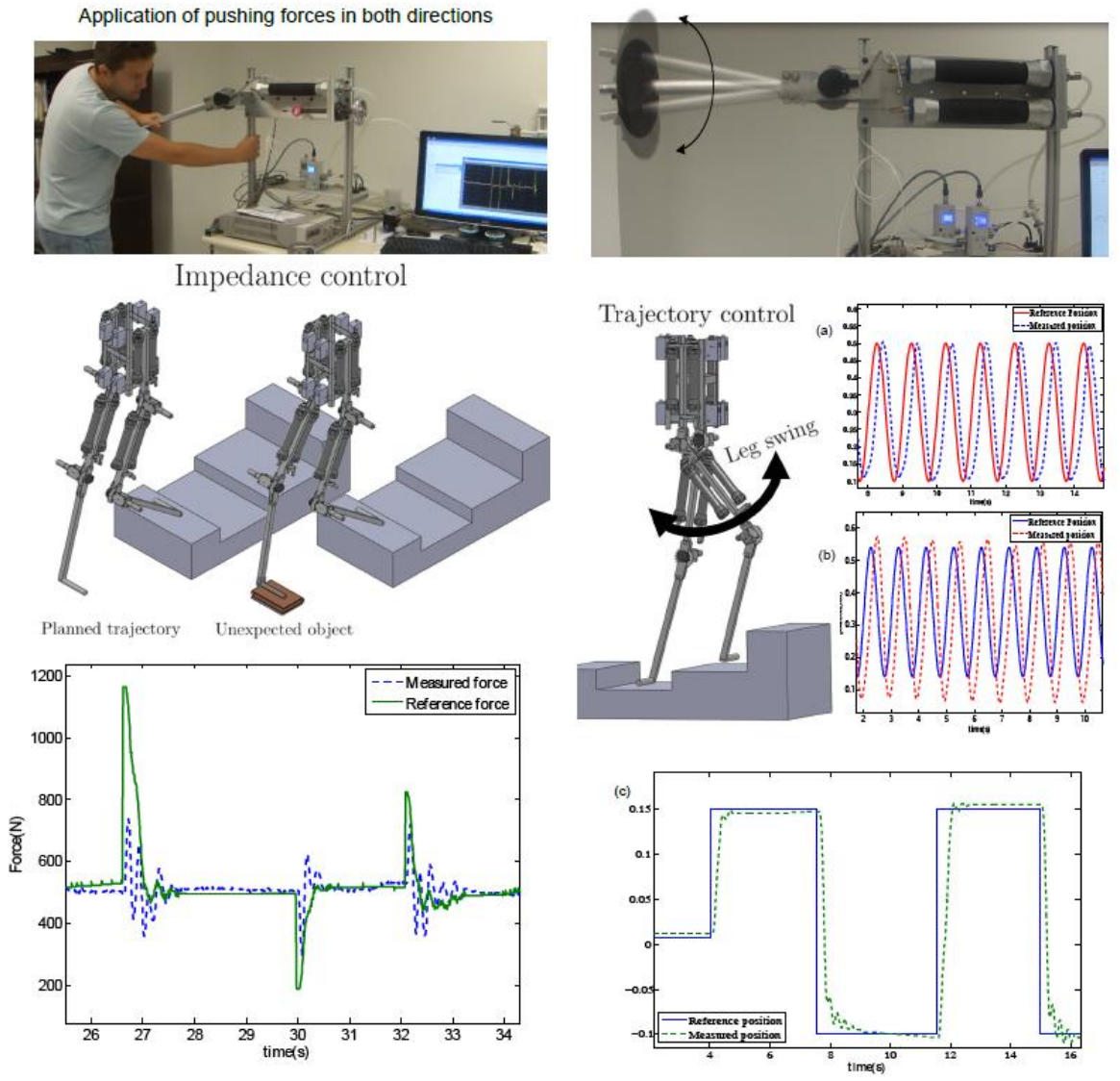

Figure 10: (LEFT) Behavior of the robot leg against impact forces: While commanding a reference force in the joint, we study its response when applying high impact external forces. This experiment could emulate a robotic leg colliding with an object. (RIGHT) Position Control: Three different experiments were performed to test the pneumatic joint tracking positions based on a force interface. The two first experiments applied a sinusoidal position reference while different weights where attached to the leg; the third experiment, corresponding to the lower graph, shows the response for a stepped position signal. The upper image depicts the movements followed by the pneumatic joint when applying a sinusoidal pattern.

The first experiment (1) is depicted in figure 10. We show force interactions with a human subject based on implementing an impedance control strategy. During this experiment, we applied high impact forces to analyze the response of the controlled PMA. Note how the pneumatic joint maintains the required force even when the impacts occur. For position control through force commands (experiment (2)), different experiments were done where trajectories of the robot leg were converted into an acceleration trajectory based on a proportional-derivative control law and further transformed to torques using a compliance controller.

Also depicted in figure 10 is a comparison between the reference position applied to the end effector and the measured position for different scenarios. For the first and second scenario, the commanded signal was a sinusoidal trajectory with a bandwidth of 1.0 [Hz], while a predefined position trajectory was used for the third experiment. In the sinusoidal case, there is no noticeable tracking attenuation in the upper graph; however a delay of 0.2[s] appears on the measured position. This delay is due to the FESTO pressure regulator response and to the slow dynamics of the pneumatic muscle. For the second scenario, although the frequency is the same, we can observed a considerable attenuation due to the fact that the mass held by the leg is higher than the previous one (20 pounds against 10 pound). The lower graph shows a position tracking experiment carried by the joint. All these experiments evoke legged locomotion because such skill involves both the tracking of position trajectories and execution of force interactions, depending on the phase of the sequence (for more details on compliant control see [45]).

Experiment (3) involved the evaluation of the PAM tracking force for a predetermined “force trajectory” and a torque control. Fig. 12 shows the results of the first experiment where it can be appreciated how the measured force follows efficiently the reference force for a wide range of positions (upper-right). In all steps, the response

time was less than 1.0 [s], which is normally the bandwidth of this kind of pneumatic actuator. The torque control experiment deals with torque control when handling a heavy object (lower-right). This experiment aims at validating the capability of the joint to support the biped's body. Videos of the results can be found at http://www.youtube.com/watch?v=jONw1rcQiqM. The results are shown in figure 11.

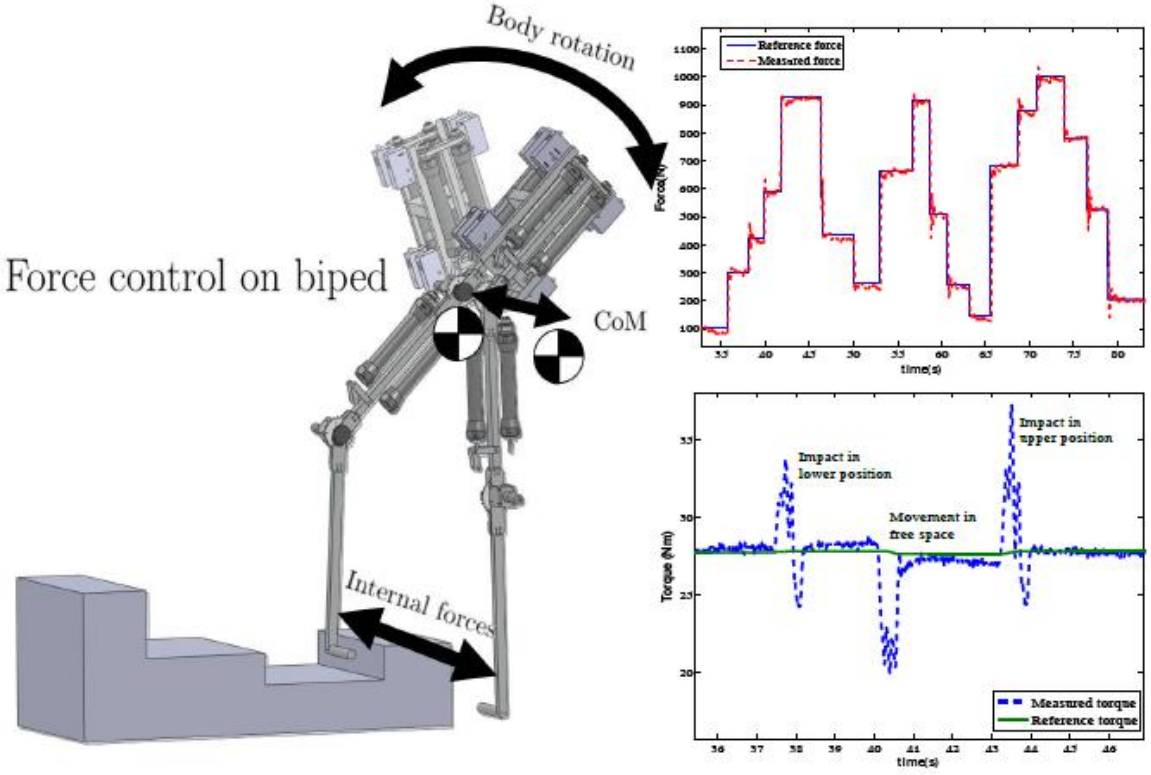

Figure 11: Force/Torque control: On the upper-right, the experiment shows a precise tracking of a force profile. It evokes some of the conditions encountered during walking, e.g. regulation of internal forces between limbs in contact (left). On the lower-right, a reference of torque is maintained by the pneumatic joint while torque disturbances where applied by a user.

The last experiment (4) is shown in Figure 12 demonstrating precise torque control of a very heavy load. The torque of the joint is controlled to compensate for the weight of the limb and the load. A user applies small forces with his hand and in

response, the joint changes its positions. The effect is the sensation of a weightless mass, despite the heavy load carried by the joint. For this experiment, the control law applied was

$$F_{1_d} = W_r \cos(\theta) \frac{r_g g}{r_0} \qquad (17)$$

where r_g is the vector to the gravity center of the robot limb (from the center of the robot joint), W_r is the estimated leg weight and g is the gravity acceleration. F_{1d} is later used as reference for the force controller implemented in fig. 7.

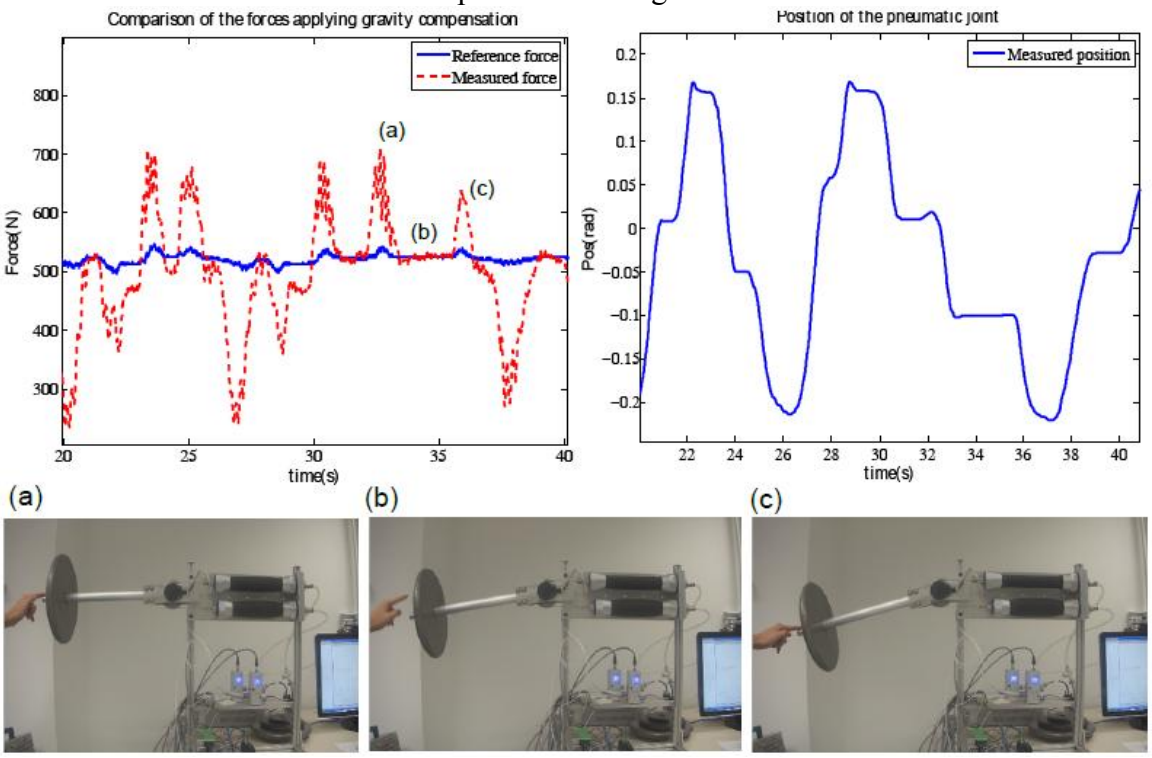

Figure 12: Gravity Compensation: A torque is commanded to compensate for the weight of a heavy load of 12[kg] for a varying position. This situation is similar to holding a leg in the air with low gains. In (a), (b) and (c) we show the sequence of movements of the heavy load upon small contact interactions with a user. Notice that the spikes correspond to the external pushes.

VII. CONCLUSIONS

Developing a new compliant joint is the first step towards creating a planar legged robot capable of walking in very rough terrains. By learning the non-linear model of the muscle system we can apply sophisticated control strategies. In particular, we have implemented force feedback and pressure compliant control with a feed-forward element of the nonlinear dynamics. Enabling the control of compliant behaviors is necessary for validating the joint capabilities for locomotion. In particular, compliance is needed to handle unexpected contacts and control internal tensions between the legs. By using high capacity force actuators, we approach the performance of the human knee during rough locomotion. However, we still under perform the capabilities of the human knee in terms of force output and range of motion. Therefore, to achieve the desired biped behaviors, we will need to resort to a lightweight robot structure that can be handled by the current actuator setup or increase the number of muscles per joint.

In the experimental section, we have shown the capabilities of the muscle to control position and torques using a common compliance interface. The results displayed by the controlled muscle system showcase its capability to lift very heavy loads and to carry out an effective torque and position tracking task—through a force interface. They also show the capacity of the joint to adapt to situations where high impact forces occur or when we need to maintain forces for a wide range of movements. However, several limitations remain to be addressed such as delayed response and limited bandwidth. To address these limitations, we plan to develop a more sophisticated nonlinear robust dynamic controller based on the muscle dynamics that relies less in quasi-static approximations.

Bibliography

[1] H. Ritter, G. Sagerer, R. Dillmann, and M. Buss, Human Centered Robot Systems. Springer, 2009.

[2] T. Y. Choi and J. Lee, "Control of manipulator using pneumatic muscles for enhaced safety," IEEE Trans. on Industrial Electronics, vol. 57(8), pp. 2815–2825, 2010.

[3] B. Ugurlu and A. Kawamura, "Zmp-based online jumping pattern generation for a one-legged robot," IEEE Trans. on Industrial Electronics, vol. 57(5), pp. 1701–1709, 2010.

[4] S. Davis, N. Tsagarakis, J. Canderle, and D. G. Caldwell, "Enhaced modellind and performance in braided pneumatic muscle actuators," Int. J. of Robotics Research, vol. 22, pp. 213–227, 2003.

[5] Z. Wu, M. Campbell, and B. Fernandez, "Bond graph based automated modeling for computer-aided design of dynamic systems," ASME Journal of Mechanical Design, vol. 140, no. 4, pp. 155–193, 2008.

[6] I. Kato, Y. Mori, and T. Masuda, "Pneumatically powered artificial legs walking automatically under various circumstances," in 4th International Conference on External Control of Human Extremities, May 1972, p. 458470.

[7] B. Verrelst, R. V. Ham, B. Vanderborght, J. Vermeulen, D. Lefeber, and F. Daerden, "Exploiting adaptable passive behaviour to influence natural dynamics applied to legged robots," Robotica, vol. 23(2), pp. 149–158, 2005.

[8] G. Spampinato and G. Muscato, Climbing and Walking Robots. Springer Berlin Heidelberg, 2006, no. 4, ch. Control Architecture and Walking Strategy for a Pneumatic Biped Robot, pp. 269–276.

[9] T. Y. Choi, S. Jin, and J. J. Lee, "Implementation of a robot actuated by artificial pneumatic muscles," in SICE-ICASE International Joint Conference, 2006, pp. 4733–4737.

[10] K. Hosoda, T. Takuma, and A. Nakamoto, "Design and control of 2d biped that can walk and run with pneumatic articial muscles," in Proceedings of the IEEE-RAS International Conference on Humanoid Robots, Genoa, Italy, December 2006, pp. 284–289.

[11] K. Tsujita, T. Inoura, T. Kobayashi, and T. Masuda, "Adaptive locomotion control of a legged robot with pneumatic actuators," in IEEE/RSJ International Conference on Robotics and Biometrics, 2007, pp. 1218–1223.

[12] D. B. Reynolds, D. W. Repperger, C. A. Phillips, and G. Bandry, "Modeling the dynamic characteristics of pneumatic muscle," Ann. Biomed. Eng., vol. 32(3), p. 310317, 2003.

[13] I. Sardellitti, G. Palli, N. Tsagarakis, and D. G. Caldwell, “Antagonistically actuated compliant joint: Torque and stiffness control,” in 2010 IEEE/RSJ International Conference on Intelligent Robots and Systems, 2010, pp. 13–18.

[14] B. Tondu and P. Lopez, “Modeling and control of mckibben artificial muscle robot actuators,” Control Systems Magazine, IEEE,, vol. 20(2), pp. 15–38, 2000.

[15] D. G. Caldwell, G. A. Medrano-Cerda, and M. Goodwin, “Control of pneumatic muscle actuators,” IEEE Control Systems, pp. 40–48, 1995.

[16] C. P. Chou and B. Hannaford, “Measurement and modeling of mckibben pneumatic artificial muscles,” IEEE Transactions on Robotics and Automation, vol. 12(1), pp. 90–102, 1996.

[17] A. Sanchez, V. Mahout, and B. Tondu, “Nonlinear parametric identification of a mckibben artifical pneumatic muscle using flatness property of the system,” in IEEE International Conference on Control Applications, 1998, pp. 70–73.

[18] G. K. Klute and B. Hannaford, “Measurement and modeling of mckibben pneumatic artificial muscles,” J. Dyn. Sys., Meas., Control, pp. 383–386, 2000.

[19] B. S. Kang, C. S. Kothera, B. K. S. Woods, and N. M. Wereley, “Dynamic modeling of mckibben pneumatic artificial muscles for antagonistic actuation,” in Proc. Int. Conf. Robotics and Automation (ICRA 2009), May 2009, pp. 182–187.

[20] R. Ramasamy, M. Juhari, M. Mamat, S. Yaacob, N. M. Nasir, and M. Sugisaka, “An application of finite element modelling to pneumatic artificial muscle,” American Journal of Applied Sciences, vol. 2(11), pp. 1504–1508, 2005.

[21] J. Sarosi, T. Szepe, and J. Geyeviki, “Approximation algorithm for the force of pneumatic artificial muscles,” in Factory Automation 2010, April 2010.

[22] T. Noritsugu and T. Tanaka, “Application of rubber artificial muscle manipulator as a rehabilitation robot,” IEEE/ASME Transactions on Mechatronics, vol. 2, p. 259267, 1997.

[23] B. Tondu, V. Boitier, and P. Lopez, “Naturally compliant robot-arms actuated by mckibben artificial muscles,” in In Proc. IEEE Int. Conf. on Systems, Man and Cybernetics, 1994, p. 26352640.

[24] D. Cai and H. Yamaura, “A sliding mode controller for manipulator driven by artificial muscle actuator,” in Electronics and Communications in Japan, vol. 3(86,11), 2003, pp. 57–64.

[25] M. Hamerlain, “An anthropomorphic robot arm driven by artificial muscles using a variable structure control,” in Electronics and Communications in Japan In Proc. IEEE/RSJ Int. Conf. on Intelligent Robots and Systems, vol. 1, 1995, pp. 550–551.

[26] T. Thanh and K. Ahn, "Nonlinear pid control to improve the control performance of 2 axes pneumatic artificial muscle manipulator using neural network," IEEE/ASME Transactions on Mechatronics, vol. 16, p. 577587, 2006.

[27] H. Aschemann and D. Schindele, "Sliding-mode control of a high-speed linear axis driven by pneumatic muscle actuators," IEEE Trans. Ind. Electron., vol. 55(11), p. 38553864, 2008.

[28] F. Anderson and M. Pandy, "A dynamic optimization solution for vertical jumping in three dimensiosn," Computer Methods in Biomechanics and Biomedical Engineering, vol. 2, pp. 201–231, 1999.

[29] N. Zheng, G. Fleisig, R. Escamilla, and S. Barrentine, "An analytical model of the knee for estimation of internal forces during exercise," Journal of Biomechanics, vol. 31, no. 1998, pp. 963–967, 1998.

[30] K. Löfler, M. Gienger, and F. Pfeiffer, "Sensors and control concept of a biped robot," IEEE Trans. on Industrial Electronics, vol. 51(5), pp. 972–980, 2004.

[31] J. Gamez Garcia, J. Gomez Ortega, A. Sanchez Garcia, and S. Satorres Martinez, "Robotic software architecture for multisensor fusion system," IEEE Trans. on Industrial Electronics, vol. 56(3), pp. 766–777, 2009.

[32] H. Paynter, Analysis and Design of Engineering Systems. Cambridge, Mass.: MIT Press, 1961.

[33] D. C. Karnopp, D. L. Margolis, and R. C. Rosenberg, System Dynamics, A Unified Approach, 2nd ed. New York, New York: Wiley-Interscience, 1990.

[34] B. O. B. Jean U Thoma, B Ould Bouamama, Modelling and Simulation in Thermal and Chemical Engineering: A Bond Graph Approach. Berlin, Germany: Springer, 2000.

[35] J.-D. Filippo, M. Delgado, C. Brie, and H. Paynter, "A survey of bond graphs : Theory, applications and programs," Journal of the Franklin Institute, vol. 328 (5-6), pp. 565–606, 1991.

[36] P. C. Breedveld, Physical systems theory in terms of bond graphs. Twente, The Netherlands: Twente University, 1954.

[37] B. Fernández, A. Prabhudesai, V. Murty, R. Gupta, and W. Chang, "Neurobondgraphs – modeling environment of nonlinear dynamic systems using neural networks and bond graphs," in Winter Annual Meeting of ASME, 1992.

[38] B. Fernández, A. G. Parlos, and W. K. Tsai, "Nonlinear dynamic system identification using artificial neural networks (anns)," in Proc. Int. Joint Conference on Neural Networks, Seattle, WA, Nov. 10-13 1990.

[39] V. Murty, Sreedhar, R., and B. Fernández, "Sparse neural networks for system identification," in World Congress on Neural Networks, Portland, OR, Jul. 11-15 1993.

[40] V. Murty and B. Fernández, "Dynet – dynamic network," in Artificial Neural Networks in Engineering, St. Louis, MO, Nov. 2-5 1993.

[41] S. Kajita, M. Morisawa, K. Harada, K. Kaneko, F. Kanehiro, K. Fujiwara, and H. Hirukawa, "Biped walking pattern generator allowing auxiliary zmp control," in Intelligent Robots and Systems, 2006 IEEE/RSJ International Conference on, October 2006, pp. 2993–2999.

[42] M. Raibert, Legged Robots that Balance. MIT Press, Cambridge, Ma., 1986.

[43] T. McGeer, "Passive dynamic walking," The International Journal of Robotics Research, vol. 9, no. 2, pp. 62–68, 1990.

[44] M. Spong, J. Holm, and D. Lee, "Passivity-based control of bipedal locomotion," Robotics Automation Magazine, IEEE, vol. 14, no. 2, pp. 30 –40, june 2007.

[45] L. Sentis, J. Park, and O. Khatib, "Compliant control of multi-contact and center of mass behaviors in humanoid robots," IEEE Transactions on Robotics, vol. 26, no. 3, pp. 483–501, June 2010.